

# Organic molecules on the surface of water droplets - an energetic perspective

Jochen S. Hub,<sup>a‡</sup> Carl Caleman,<sup>b§</sup> and David van der Spoel<sup>\*a</sup>

Received Xth XXXXXXXXXXXX 20XX, Accepted Xth XXXXXXXXXXXX 20XX

First published on the web Xth XXXXXXXXXXXX 200X

DOI: 10.1039/b000000x

The solubility of organic molecules is a well established property, founded on decades of measurements, the results of which have been tabulated in handbooks. Under atmospheric conditions water droplets may form containing small amounts of other molecules. Such droplets typically have a very large area to volume ratio, which may shift the solvation equilibrium towards molecules residing on the droplet surface. The presence of organic molecules on droplet surfaces is extremely important for reactivity – it is well established that certain chemical reactions are more prevalent under atmospheric conditions than in bulk. Here we present a thermodynamic rationalization of the surface solvation properties of methanol, ethanol, propanoic acid, n-butylamine, diethyl ether, and neopentane based on potential of mean force (PMF) calculations - we have previously demonstrated that an energetic description is a very powerful means of disentangling the factors governing solvation (Caleman *et al.*, Proc. Natl. Acad. Sci. U.S.A. **108** (2011) 6838-6842). All organic molecules investigated here are preferentially solvated on the surface of the droplets rather than in the inside, yet the magnitude of surface preference may differ by orders of magnitude. In order to dissect the energetic contributions that govern surface preference, we decompose the PMF into enthalpic and entropic components, and, in a second step, into contributions from water-water and solute-water interactions. The analysis demonstrates that surface preference is primarily an enthalpic effect, but the magnitude of surface preference of solutes containing large apolar groups is enhanced due to entropy. We introduce an analysis of the droplet PMFs that allows one to extrapolate the results to larger droplets. From this we can estimate the solubility of the solutes in water droplets, demonstrating that the solubility in droplets can be orders of magnitude larger than in bulk water. Our findings have implications for understanding the process of electrospray ionization, an important technique in biological mass spectrometry, since our work strongly suggests that in equilibrium biomolecules would be adsorbed on the droplet surface as well.

## 1 Introduction

Water in the atmosphere plays an important role in the climate on earth and is highly involved in the atmospheric chemistry. Oceans cover over 70% of the surface of earth and water in some form (vapor, aerosols, liquid or ice) can be found anywhere in the troposphere, the atmospheric layer closest to the surface of earth<sup>1</sup>. Measurements have shown that atmospheric aerosols include a significant portion of organic material<sup>2–7</sup>. These aerosols originate from surfaces of oceans, seas or lakes and are ejected into the air through bubbles, which are converted into a fine spray as they burst<sup>8,9</sup>. Reactions at surfaces containing organic films are often different from those in the bulk, and water-air interfaces in the atmosphere provide a

competent reaction environment<sup>10,11</sup>, although not necessarily better than bulk water<sup>12</sup>. The exact composition of the surface is therefore relevant to many of the chemical reactions that occur in the atmosphere and that affect climate<sup>13</sup>. In addition, organic molecules serve as cloud condensation nuclei<sup>14–16</sup>, and nucleation due to sulphuric acid particles is enhanced by the presence of organic compounds<sup>17–19</sup>. Therefore, the effect of organic layers on water aerosols in the atmosphere has been the subject of research for several decades, for reviews on the subject see references<sup>20–22</sup>.

Despite the significance of surface solvation, little is known about the thermodynamic driving forces underlying the preference of organic molecules for the water/vapor interface. Therefore, we present here a systematic analysis of the energies that are involved in the solvation of solutes in a small water droplet. We investigate the surface preference of six molecules of different size and bulk solvation energies: methanol, ethanol, propanoic acid, n-butylamine, diethyl ether, and neopentane. Except for neopentane, these solutes are amphiphilic —containing both hydrophobic and hydrophilic parts—, promoting the surface preference of these

<sup>a</sup> Department of Cell and Molecular Biology, Box 596, SE-75124, Uppsala, Sweden. Fax: 46 18 ; Tel: 46 18 471 4205; E-mail: [spoel@xray.bmc.uu.se](mailto:spoel@xray.bmc.uu.se)

<sup>b</sup> Center for Free-Electron Laser Science, DESY, Notkestraße 85, DE-22607 Hamburg, Germany

<sup>‡</sup> Present address: Georg-August-University Göttingen, Institute for Microbiology and Genetics, Justus-von-Liebig-Weg 11, 37077 Göttingen, Germany

<sup>§</sup> Present address also: Department of Physics and Astronomy, Uppsala University, Box 516, SE-751 20 Uppsala, Sweden

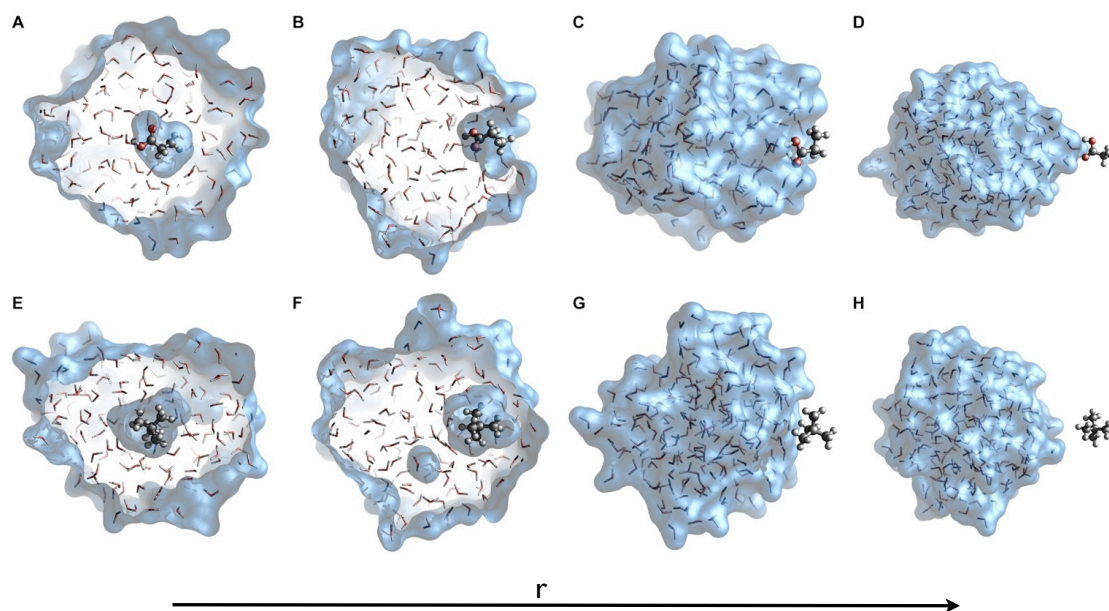


**Fig. 1** Solvation of (A-D) propanoic acid and (E-H) neopentane at different positions in a droplet of water. Positions in the direction of the arrow for  $r = 0.15, 0.6$ , at the minimum of the respective PMF, and at  $1.7\text{nm}$ , where  $r$  denotes the center of mass distance between water and solute.

solutes. Neopentane, in contrast, represents a purely hydrophobic solute. Although neopentane is to some extent stabilized at the water surface as well, we included neopentane in this study in order to compare the thermodynamics of surface solvation to the well-established thermodynamics of the hydrophobic effect, that is the increase in free energy upon the transfer of a hydrophobic molecule from a non-aqueous phase into bulk water<sup>23,24</sup>. At room temperature, the free energy change upon that transfer is mainly due to entropy, whereas the change in enthalpy is approximately zero<sup>25</sup>.

Mixing of liquids is determined by a subtle balance of enthalpy and entropy. Even though molecules like methanol and water can be mixed over the whole concentration range, the methyl groups still tend to cluster to some degree in methanol solutions<sup>26</sup>. Dielectric relaxation measurements of a number of alcohol/water mixtures have revealed mixing to be a complex function of alcohol concentration<sup>27–30</sup>. Molecular simulation of such mixtures reproduces most features of these mixtures at least qualitatively<sup>31,32</sup>. A key feature that was found in such simulations is that all alcohols (methanol, ethanol, and 1-propanol were tested) have elevated concentrations at the air/water surface<sup>33</sup>, due to the hydrophobic effect. The excess surface tension of alcohol/water mixtures was predicted by these simulations to deviate less from ideality than what is found experimentally, a typical problem in classical non-polarizable force fields. Further studies reported effects of an organic surfactants on ion distributions at the air/water inter-

face<sup>34</sup>, and the adsorption of water on organic surfaces has been addressed<sup>35</sup>.

Here we use droplets rather than 2-dimensional periodic surfaces, because small droplets are more relevant from an atmospheric chemistry perspective, but also because they provide a means to compute exact potentials of mean force (PMFs) since all interactions can be taken into account explicitly. In previous studies of the evaporation from pure water droplets<sup>36</sup> and water droplets containing ions<sup>37,38</sup> we have studied evaporation properties as well as ion PMFs. The results of these simulations were corroborated by Otten *et al.* recently<sup>39</sup>. From microsecond simulations using simple water models like the simple point charge model<sup>40</sup> we were able to confirm that evaporation from droplets stops if the temperature drops to below  $220\text{K}$ <sup>36</sup>, however, such low temperatures are found only in the tropopause, at the border between the stratosphere and the troposphere where the air is nearly completely dry. This implies that evaporation and condensation are important under all relevant atmospheric conditions and that models reproducing these features need to be applied<sup>36</sup>.

For this study of organic molecules on droplets, a non-polarizable force field was used. The choice of force field was validated by computing the Gibbs energy of hydration ( $\Delta G_{\text{hyd}}$ ) as well as key properties of liquids composed of the organic molecules using the OPLS/AA force field<sup>41</sup> in combination with three different water models (SPC<sup>40</sup>, SPC/E<sup>42</sup> and TIP3P<sup>43</sup>) as well as the generalized amber force field<sup>44</sup> in

combination with the TIP3P water model<sup>43</sup>. We then selected the model that performed best in comparison to experimental data.

## 2 Methods

### 2.1 Gibbs energy of hydration

In order to validate the choice of force field for the potential of mean force calculations, we performed free energy perturbation calculations using thermodynamic integration (TI)<sup>45</sup>.  $\Delta G_{\text{hyd}}$  was computed in a box of water (not in the water droplet). The TI was conducted in three steps, following the protocol of Shirts *et al*<sup>46</sup>:

- (i) Turn off all interactions of the solute in vacuum;
- (ii) turn on Lennard-Jones interactions between solute and solvent in a box of water;
- (iii) turn on in addition the Coulomb interactions between the solute and water.

Steps (ii) and (iii) were simulated in a cubic simulation box of 511 water molecules, and step (i) in an simulation box of the same volume (27 nm<sup>3</sup>) but containing the solute only. The transitions were carried out along an alchemical reaction coordinate  $\lambda$ , where  $\lambda = 0$  and  $\lambda = 1$  correspond to the initial and final states, respectively. Step (i), (ii), and (iii) were decomposed into 21 equally spaced  $\lambda$ -steps, respectively, and each  $\lambda$ -step was simulated for 550 ps, the first 50 ps of which was discarded for equilibration. All simulation parameters were identical to the other simulations, except that the temperature was controlled via a stochastic dynamics integration scheme ( $\tau = 0.1$  ps), and that step (i) was simulated at constant volume. Free-energy differences for each step were subsequently computed by integrating  $\langle \partial \mathcal{H} / \partial \lambda \rangle$  from  $\lambda = 0$  to  $\lambda = 1$ . Here,  $\langle \cdot \rangle$  denotes the average computed from the respective trajectory, where  $\mathcal{H}$  is the Hamiltonian of the system.  $\Delta G_{\text{hyd}}$  is given by sum of the free energy differences of the three steps. Statistical errors for  $\langle \partial \mathcal{H} / \partial \lambda \rangle$  were computed using binning analysis, which subsequently yield the error for  $\Delta G_{\text{hyd}}$  via Gaussian error propagation.

### 2.2 Selection of models

Four different combinations of force field and water model were used. OPLS/AA<sup>41,47,48</sup> was combined with SPC<sup>40</sup>, the extended simple point charge model (SPC/E)<sup>42</sup> and the four point transferable intermolecular potential (TIP4P)<sup>43</sup>. The generalized Amber force field (GAFF)<sup>44</sup> was used in combination with the three point transferable intermolecular potential (TIP3P)<sup>43</sup>. The final choice of model is described in the results section.

### 2.3 PMF calculations

Potential of mean forces (PMFs) were computed similar to the protocol in ref.<sup>38</sup> using constrained molecular dynamics simulations. Along the reaction coordinate  $r$ , that is the distance of the center of mass (COM) of the solute and the COM of the water droplet, 59 positions were selected in the range  $0.15 \text{ nm} \leq r \leq 2 \text{ nm}$ , with a distance of 0.025 nm between adjacent positions in the range of  $0.6 \text{ nm} \leq r \leq 1.65 \text{ nm}$ , and a distance of 0.05 nm between all other adjacent positions.

Fig. 1 illustrates the concept that shows how the molecules are positioned when the energies are computed. For each position, the respective solute was placed into the structure and the distance between solute COM and droplet COM was constrained for the following simulations. The orientation of the solute was not restrained, allowing the simulations to average over all orientations of the solute. Overlaps between solute and water atoms were removed by gradually switching on Lennard-Jones interactions between solute and water within 1000 simulation steps, using soft-core Lennard-Jones potentials and a stochastic dynamics integration scheme. Thereafter, the energy of each structure was minimized and each system was simulated for 100 ns. After removing the first 0.5 ns of each trajectory for equilibration, the PMFs were computed by integration of the mean force. Statistical errors for all properties were computed by binning analysis<sup>49</sup>, and the errors in the PMFs using standard error propagation. An analytical entropy correction for spherical systems was applied to the PMFs<sup>50</sup>, according to:

$$\Delta S_{r_0}(r) = k_B \ln \left( \frac{r}{r_0} \right)^2 \quad (1)$$

where  $k_B$  is the Boltzmann factor and  $r_0$  is a reference distance.  $r_0$  was chosen such that the average of the PMF within  $r < 0.5 \text{ nm}$  equals zero, yielding the PMFs relative to the inside of the droplet.

$\Delta H(r)$  was computed as the average potential energy of the system in each simulation since the volume is constant and the temperature is controlled and therefore a constant contribution from the temperature does not affect the relative enthalpies. The entropic contribution the PMFs was computed as

$$-T\Delta S(r) = G(r) - H(r). \quad (2)$$

The interaction energies were computed as the average of the sum of the respective Lennard-Jones and Coulomb interactions. Statistical errors of the energies were likewise derived by binning analysis<sup>49</sup>. We would like to stress that the thermodynamic function  $G(r)$  is valid only for the system simulated here, and the numbers can not be compared directly to, for instance, an infinite slab system.

All simulations were carried out using the GROMACS simulation software<sup>51,52</sup>. Topology files as well as structure

files of the solute molecules will be deposited on the GRO-MACS Molecule & Liquid database<sup>53</sup> which is available at <http://virtualchemistry.org>. Details about how the structures and the topologies were generated, as well as how well the force field performs for such molecules in the liquid phase were presented recently by Caleman *et al.*<sup>54</sup>

Newton's equation of motion were solved using the Leap-Frog integration scheme<sup>55</sup> with a time step of 2 fs. The temperature was controlled at 293.15 K using a stochastic dynamics integrator ( $\tau = 0.1$  ps)<sup>56</sup>. No cut-offs were applied to the Lennard-Jones or Coulomb interactions, and the droplet was simulated in vacuum (without periodic boundary conditions). The SETTLE algorithm was used to constrain the water molecules<sup>57</sup>, and bond lengths of the solutes were constrained by the LINCS algorithm<sup>58</sup>. Because we simulated at room temperature, individual water molecules would frequently evaporate from the droplet surface, which would lead to an ill-defined droplet center of mass (COM). To avoid such evaporation, we applied a spherical flat-bottom quadratic potential acting on the water. That potential was implemented as an additional force

$$F(r) = -k/2(r - r_{fb})^2 H(r - r_{fb}) \quad (3)$$

pointing towards the COM of the droplet, where  $k = 500 \text{ kJ mol}^{-1} \text{ nm}^{-2}$  denotes the force constant,  $r_{fb} = 1.4$  nm the radius of the sphere around the COM without any additional force, and  $H$  the Heaviside step function. We found that the average flat-bottom potential is  $< 2.2$  kJ/mol for simulations of propanoic acid and  $< 1$  kJ/mol for all other simulations, much smaller than the alterations of the other energies analyzed here. Therefore, a specific choice for  $k$  is not expected to affect the results.

## 2.4 Solute fraction at the droplet surface

The fraction of solutes located at the surface of a droplet of arbitrary size was estimated from the PMFs. Because that estimate is based on single-solute calculations, the result is only valid at low solute concentration. At higher solute concentration, multiple solutes may stabilize each other at the surface or in the bulk, leading to an enhanced or reduced solute fraction at the surface, respectively.

The PMFs at the surface were assumed to be approximately independent of the droplet radius. Thus, the PMFs  $\Delta G(r)$  for the simulated droplet (surface radius  $r_s^* = 1.1$  nm) were applied to approximate the PMF for an arbitrary droplet radius  $r_s$  via  $\Delta G'(r; r_s) = \Delta G[r - (r_s - r_s^*)]$ . The surface layer  $r_1 < r < r_o$  was defined using  $r_1 = r_s - 0.5$  nm and  $r_o = r_s + 0.6$  nm. Here,  $r_1$  and  $r_o$  were motivated from the shape of the minima of the PMFs (see Results), yet the specific choice hardly affects the results. The average number of molecules in the surface layer

$N_s$  is given by

$$N_s(r_s) = C_b \int_{r_1}^{r_o} 4\pi r^2 \exp[-\Delta G(r; r_s)/k_B T] dr. \quad (4)$$

Here,  $C_b$  denotes the concentration of the solute in the bulk, where the PMF is defined to zero, and  $T$  is the temperature. Likewise, the number of molecules in the bulk is  $N_b(r_s) = 4\pi r_1^3 C_b/3$ , and the fraction of molecules on the surface equals  $N_s(r_s)/[N_s(r_s) + N_b(r_s)]$ . Note however, that the above analysis is valid only at concentrations low enough such that the solute molecules do not interact.

A intuitive number to quantify to surface preference of a solute is given by the radius  $r_{eq}$  that would lead to an equal fraction of solutes in the bulk and on the surface, that is  $N_s(r_{eq}) = N_b(r_{eq})$ . Thus, an increasing  $r_{eq}$  quantifies an increasing surface preference of the solute. If the radius of the droplet is much larger than the thickness of the surface layer where  $\Delta G$  deviates from zero,  $r_{eq}$  can be approximated by

$$r_{eq} = 3 \int_{r_1}^{r_o} \exp[-\Delta G(r)/k_B T] dr. \quad (5)$$

That approximation is expected to hold if the solute is much smaller than the droplet.

## 3 Results

### 3.1 Selection of force field models

In order to select an accurate model we computed the Gibbs free energy of hydration for the six molecules, using four different force field/water model combinations. The results are given in Table 1. All models reproduce the correct order of  $\Delta G_{hyd}$ , within the precision of the calculations. The root mean square deviation from experiment were lowest for both the combinations of OPLS/AA with SPC and GAFF with TIP3P. Furthermore, properties of the pure liquids were computed (see Supporting Information), following the recipe from our recent benchmark study<sup>54</sup>. Density as well as enthalpy of vaporization were reproduced slightly better for the OPLS/AA liquids and therefore we selected the OPLS/AA force field in combination with the SPC water model for the following calculations.

### 3.2 Droplet PMFs

Figure 3A presents the PMFs for the six solutes, with the reaction coordinate  $r$  corresponding to the distance between the center of mass (COM) of the water droplet and the COM of the solute. All PMFs were defined to zero in the inside of the droplet and thus quantify the free energy difference with respect to the bulk water. The Gibbs dividing surface, that is

**Table 1** Gibbs energy of hydration  $\Delta G_{\text{hyd}}$  (kJ/mol) at 300 K for six molecules using four different force fields / water model combinations. The root mean square deviation (RMSD) from experiment is given to distinguish the quality of the models. Experimental data were taken from the Minnesota Solvation Database<sup>59</sup>.

Molecule	Exper.	OPLS/AA		GAFF	
		SPC/E	SPC	TIP/4P	TIP3P
Methanol	-21.4	-19.0±0.3	-18.7±0.5	-19.9±0.5	-19.0±0.4
Ethanol	-21.0	-18.5±0.5	-18.9±0.4	-19.2±0.4	-16.4±0.4
Propanoic acid	-27.0	-20.3±0.6	-22.6±0.6	-20.4±0.5	-26.5±0.6
Diethyl ether	-7.4	-0.9±0.6	-1.8±1.0	-1.4±0.6	1.4±0.4
N-butylamine	-17.9	-10.3±0.6	-10.8±0.5	-11.7±0.5	-14.8±0.5
Neopentane	10.5	11.9±0.7	10.0±0.7	11.7±0.9	9.2±0.5
RMSD		5.0	4.2	4.5	4.2

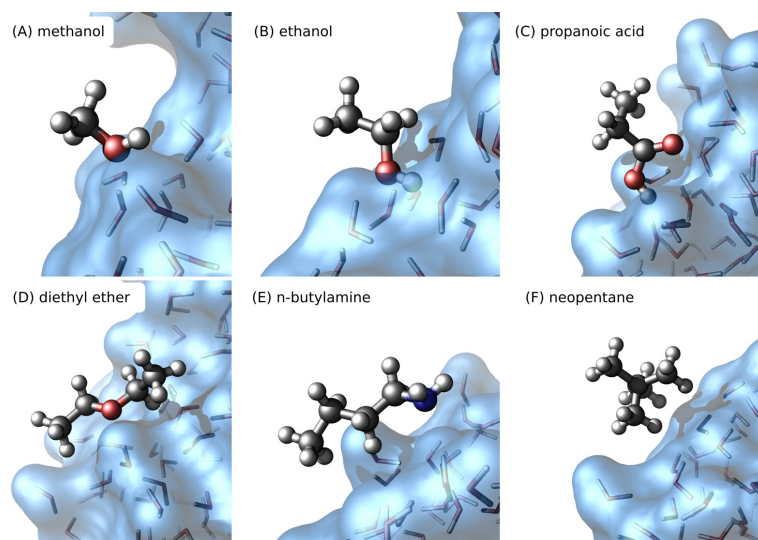


**Fig. 2** Close ups of surface solvation geometries for the six molecules. The solute positions correspond to the minimum of the respective PMF.

the surface of the droplet in the absence of the solute, is indicated as a grey broken line in Fig. 3A. All PMFs show a marked minimum near the droplet surface, varying between -6 kJ/mol (methanol) to -28 kJ/mol (neopentane). Because the PMFs  $\Delta G(r)$  translate into the solute concentration along  $r$  via  $C(r) = C_b \exp(-\Delta G(r)/k_B T)$  where  $C_b$  denotes the concentration in the bulk, these minima quantify the surface preference of the solutes. Typical simulation snapshots of the water droplet with propanoic acid or neopentane along the reaction coordinate  $r$  are also visualized in Fig. 1.

Figure 2 shows the six molecules at representative configurations at the respective PMF minima. As expected, all solutes adopt a conformation with their polar side facing the water in order to form favorable polar interactions (except neopentane obviously). In addition, if compatible with the geometry of the solute, solutes tend to “lay down” on the surface in order to form Van-der-Waals contacts between hydrophobic solute

groups and water (Fig. 2D/E and Fig. 1C.).

The PMFs alone may not provide an intuitive measure for surface preference. In particular, the fraction of molecules that are dissolved at the droplet surface is not obvious from the PMFs. Therefore, Fig. 4 presents the average fraction of molecules dissolved at the surface versus the surface radius  $r_s$  of a water droplet (see Methods for details). At small  $r_s$ , i.e. large surface to volume ratio, the surface preference of all solutes is sufficiently strong to desolvate all six molecules on the droplet surface, as apparent from a surface fraction near unity. With increasing  $r_s$ , i.e. decreasing surface to volume ratio, an increasing fraction of the solutes becomes fully solvated in the bulk interior of the droplet, reflected in a decreasing surface fraction. A single intuitive number to quantify the surface preference of solutes is given by the droplet radius  $r_{\text{eq}}$  that would lead to an equal fraction of solutes on the surface and in the bulk. Hence, increasing  $r_{\text{eq}}$  indicates a more pronounced

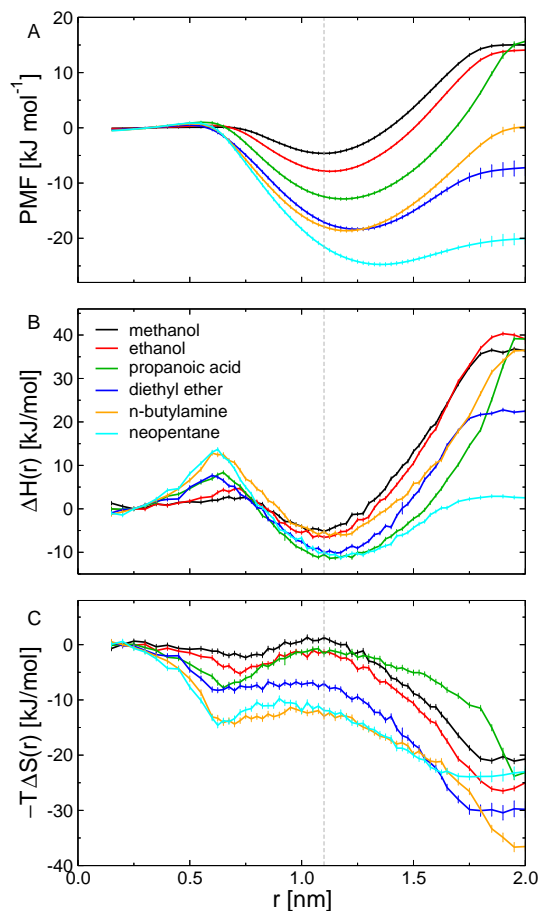


**Fig. 3** PMF, enthalpy and entropy as a function of position in the water droplet for six molecule. The grey dashed line indicates the Gibbs dividing surface.

surface preference. For large droplets,  $r_{\text{eq}}$  is approximated by eq. 5, shown as circles in Fig. 4, and the surface fraction given by  $[r_s/r_{\text{eq}} + 1]^{-1}$ . For the six molecules studied here, the calculation yields for  $r_{\text{eq}}$  8.5 nm (methanol), 28 nm (ethanol), 220 nm (propanoic acid), 2.1  $\mu\text{m}$  (diethyl ether), 2.2  $\mu\text{m}$  (n-butylamine), and 32  $\mu\text{m}$  (neopentane).

### 3.3 Energetic driving forces underlying surface preference

Now that we have established the surface preference of the six solutes, we turn towards the thermodynamic (or energetic) driving forces underlying surface preference. Accordingly, we decomposed the PMFs  $\Delta G(r)$  into their enthalpic component  $\Delta H(r)$  (Fig. 3B) and entropic component (Fig. 3C), where the latter is presented as  $-T\Delta S(r)$ . In this manner, the curves in Figs. 3B and C add up to the PMFs via  $\Delta G(r) = \Delta H(r) - T\Delta S(r)$ . A number of remarkable properties of sur-

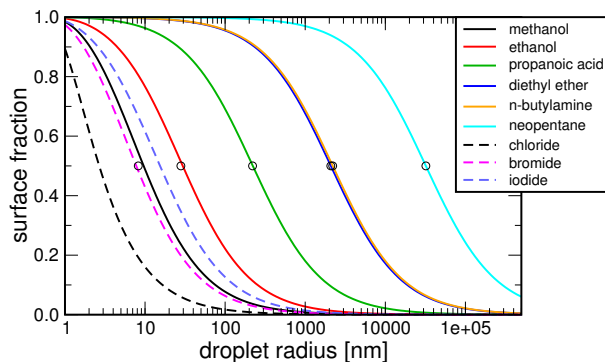


**Fig. 4** Fraction of solutes located at the water/vapor interface versus the radius of the droplet. Droplet radii  $r_{\text{eq}}$  generating an equal solute number on the surface and in the bulk are indicated as circles. Broken lines show the surface fraction of halide ions based on the PMFs in Caleman *et al.*<sup>38</sup>

face solvation can be extraction from Figs. 3B/C.

- i) All enthalpic curves (Fig. 3B) display a pronounced minimum at the surface, demonstrating that the stability at the surface is mainly an enthalpic phenomenon.
- ii) All enthalpic curves display a maximum just below the droplet surface ( $r \approx 0.6$  nm). Two typical configuration are visualized in Figs. 1B/F. The unfavorable enthalpy in such configurations can be rationalized by an increased water surface, allowing only a reduced number of water-water contacts. However, the unfavorable enthalpy at  $r \approx 0.6$  nm is nearly fully compensated by increased entropy (Fig. 3C), probably through an increased rotational freedom of water molecules. Consequently, the enthalpic barrier is reflected only in a minute hump in the PMFs (Fig. 3A).
- iii) The simulations predict zero transfer enthalpy for neopentane from vacuum ( $r = 2$  nm) to bulk, that is the positive transfer free energy of 20 kJ/mol is purely due to entropy (Fig. 3, cyan curves). That finding favorably agrees with the well-established thermodynamics of the hydrophobic effect,<sup>23,24</sup> giving faith in the simulation protocol. Accordingly, at room temperature, the increase in free energy upon that transfer (that is the hydrophobic effect) is dominated by a decrease in entropy.
- iv) Large nonpolar groups as present in neopentane, n-butylamine, and diethyl ether lead to increased entropy at the surface as compared to the bulk (Fig. 3C). Hence, an entropic effect enhances the surface preference of solutes with large nonpolar groups.

In order to understand the distinct shape of the enthalpic profiles, we have further decomposed these into water-water

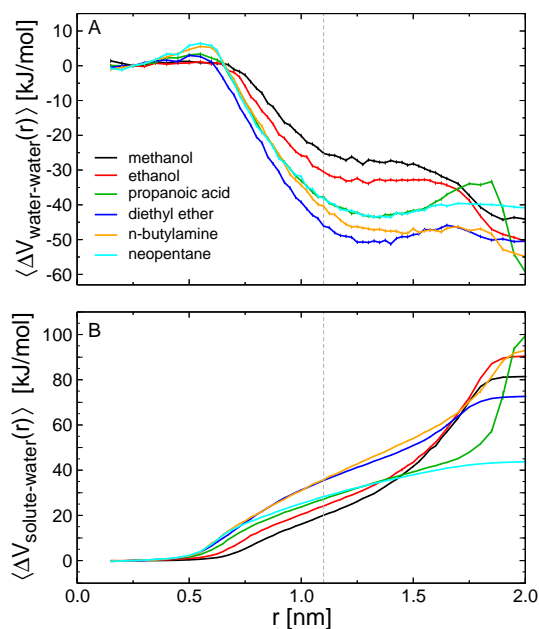


**Fig. 5** Decomposition of the enthalpic profiles into (A) water-water and (B) solute-water interaction energies for the six molecules.

(Fig. 5A) and solute-water (Fig. 5B) interaction energies. The profiles present the potential energy difference with respect to the bulk state, and the profiles in Figs. 5A and B thus add up to the curves in Fig. 3B, i.e.  $\Delta H(r) = \langle V_{\text{water-water}}(r) \rangle + \langle V_{\text{solute-water}}(r) \rangle$ . While solutes travel from the bulk to the surface, favorable water-water interactions form (become more negative, Fig. 5A). That finding reflects the fact that solutes at the surface do not disrupt water-water hydrogen bonds to the same extent as solutes in the bulk. Simultaneously, with increasing  $r$ , some solute-water interactions get lost (become more positive) with increasing  $r$  (Fig. 5B). At the surface, however, the gain in water-water interactions outweighs the loss of solute-water interactions, yielding the favorable drop in enthalpy (Fig. 3B). Only as the solute is transferred further into the vapor phase at  $r > 1.5$  nm, the loss in solute-water interactions outweighs the gain in water-water interactions, yielding an unfavorable increase in enthalpy.

To summarize the energetic analysis, the surface preference of the organic molecules studied here is predominantly an enthalpic effect. However, if the molecule contains large polar groups, the magnitude of surface preference is enhanced by the hydrophobic effect, which is driven by entropy at room temperature.<sup>23</sup> The enthalpic minimum at the surface is constituted by two different energetic contributions. Water-water interactions generate unfavorable enthalpies for solutes being in the bulk, hereby “pushing” solutes to the surface. Solute-water interactions lead to an increasing enthalpy as the solutes move from the surface into vacuum, thereby “pulling”

solutes back onto the surface, as visualized for propanoic acid in Fig. 1D.

## 4 Discussion

Hydration properties can be understood by considering the hydrophobic effect, which states that water repels nonpolar substances. The thermodynamic reason for this is dependent on both the temperature and the size of the hydrophobic particle, as reviewed in detail by Southall *et al.*<sup>23</sup> and Chandler<sup>24</sup>. For small hydrophobic molecules such as neopentane, the effect is entropy-driven at room temperature, while the effect is dominated by enthalpy near the boiling temperature of water. Likewise, as the size of the solvated molecule increases, enthalpy dominates the hydrophobic effect whereas entropy becomes less important. These observations can be understood from the hydrogen bond geometry of water around the hydrophobic solute.<sup>60</sup> At temperatures relevant for atmospheric conditions, roughly 200-300 K, the entropic contribution to the hydrophobic effect is therefore particularly important.

In contrast, we found that enthalpy stabilizes solutes at the surface of water droplets. Here, a combination of both water-water and solute-water interaction energies generates favorable enthalpies for surface configurations. Upon the transfer of solutes from the bulk to the surface, favorable water-water interactions are formed (Fig. 5A), leading to decreased enthalpy. If the solutes are further transferred from the surface into vacuum, however, solute-water interactions are lost, leading to an unfavorable increase in enthalpy (Fig. 5B). Whereas enthalpy generates the stabilizing free energy minimum at the surface, entropy can enhance the depth of the minimum, and, hence, drastically enhance the surface preference. This feature was here observed for diethyl ether, n-butylamine, and neopentane, which show increased entropy of  $\sim 10$  kJ/mol (measured in  $T\Delta S$ , Fig. 3C) for the surface state as compared to the bulk state. Hence, entropy leads to the great surface preference of solutes, we have introduced the droplet radius  $r_{\text{eq}}$  that yields an equal fraction of solutes on the surface and in the bulk. An increasing  $r_{\text{eq}}$  thus quantifies an increasing surface preference (Fig. 4).

Recently, concerns were raised whether the decomposition of enthalpy into water-water and solute-water interactions is reasonable.<sup>61</sup> As shown by Yu and Karplus 25 years ago, the change in entropy can be mathematically decomposed into contributions from water-water and solute-water interactions<sup>62</sup>,  $\Delta S(r) = \Delta S_{\text{water-water}}(r) + \Delta S_{\text{solute-water}}(r)$ . Here,  $\Delta S_{\text{water-water}}$  and  $\Delta S_{\text{solute-water}}$  are computed from integrals over ensemble averages of (derivatives of) water-water and solute-water interaction energies, respectively, and, remarkably,  $T\Delta S_{\text{water-water}}(r)$  cancels with  $\langle \Delta V_{\text{water-water}}(r) \rangle$ .<sup>62</sup> We agree that the decomposition of  $\Delta G(r)$  is thus not unequivocal

and could instead be presented as  $\Delta G(r) = -T\Delta S_{\text{solute-water}} + \langle \Delta V_{\text{solute-water}}(r) \rangle$ . However, we here suggest to decompose  $\Delta G(r)$  into components that are intuitive and, if possible, experimentally accessible. The structural interpretation of  $\Delta S_{\text{solute-water}}$  is unclear, partly because it also depends on water-water interactions through the ensemble averages, which are carried out with the total potential in the exponential Boltzmann factor. In addition, the derivation by Yu and Karplus only holds in the case of pairwise additive potentials (like those used in the present paper), but not for the polarizable models that we used previously<sup>38</sup>. In contrast to the hardly interpretable  $T\Delta S_{\text{solute-water}}$ , the water-water interaction energy  $\langle \Delta V_{\text{water-water}}(r) \rangle$  is intuitive and mainly given by the average number of water-water hydrogen bonds, and it has frequently been employed to understand the hydrophobic effect.<sup>24,63</sup>  $T\Delta S(r)$  is experimentally accessible. The decomposition used here,  $\Delta G(r) = -T\Delta S(r) + \langle \Delta V_{\text{water-water}}(r) \rangle + \langle \Delta V_{\text{solute-water}}(r) \rangle$ , is therefore useful to gain qualitative insight into surface preference.

What are the implications of these findings for atmospheric droplets? First, bulk solubilities cannot be transferred directly to droplet solubilities. Instead, favorable surface solvation can greatly enhance the solubility of solutes (if *solubility* refers to solvation both in bulk and on the surface). Let us assume that the surface layer is thin compared to the droplet radius, that is the outermost layer with solute-water contact, but where  $\Delta G(r)$  deviates from zero. Then, the solubility of a solute in the entire droplet (including bulk and surface) is given by

$$x_{\text{droplet}} = x_{\text{bulk}}(r_{\text{eq}}/r_s + 1), \quad (6)$$

where  $x_{\text{bulk}}$  denotes bulk solubility. In droplets which are small compared to  $r_{\text{eq}}$ , the surface solution thus greatly enhances the solubility of the solute, possibly by orders of magnitude.

With the observation that a large fraction of neutral molecules may be adsorbed at the surface rather than adsorbed inside the droplet (Fig. 4), follows necessarily that reactions under atmospheric conditions will be influenced by this<sup>13,64,65</sup>. For instance reactions involving bromide ions have long been known to proceed more rapidly in the atmosphere than can be expected from bulk bromide concentrations in seawater and reactions may proceed in a different manner as well<sup>66</sup>.

Finally, these findings have implications for encapsulation of biomolecules in droplets using electrospray ionization<sup>67</sup>, the technique that has facilitated mass-spectrometry. We have previously studied process of "drying" proteins in electrospray<sup>68,69</sup> and the encapsulation of proteins in lipid aggregates<sup>70-72</sup>, the Konermann group have focused on the related process of electrospray charge state distribution<sup>73,74</sup> and more recently on the effect of protein conformation on drying in electrospray<sup>75</sup>. Existing models of the electrospray process, in

particular the charge residue model<sup>76,77</sup> assume a biomolecule will be completely immersed in solvent, and it has even been suggested that this feature could be exploited for protecting biomolecules in droplets in X-ray free electron lasers<sup>78-80</sup>. However, because proteins are amphiphilic, the present study suggests that proteins in small droplets may be transferred to the surface as well and, thus, possibly expose parts of the protein to the vacuum. A recent paper by Ahadi and Konermann investigates this using a coarse-grained model<sup>75</sup>, however, it would be highly interesting to probe the determinants for bulk/surface preference of proteins in atomistic detail as well.

## Supporting information

Supporting information is available for this paper containing liquid properties for all six molecules for which PMFs were calculated.

## Acknowledgements

J.S.H. acknowledges support through a Marie-Curie Intra-European fellowship within the 7th European Community framework program. The Helmholtz Association is thanked for supporting C.C. through the Center for Free-Electron Laser Science. The Swedish Research Council is acknowledged for financial support to D.v.d.S. (2007-5671) and for a grant of computer time (SNIC 022/09-10).

## References

- 1 R. Goodly, *Principles of Atmospheric Physics and Chemistry*, Oxford University Press, Oxford, UK, 1995.
- 2 R. Duce, V. Mohnen, P. Zimmerman, D. Grosjean, W. Cautreels, R. Chatfield, R. Jaenicke, J. Ogren, E. Pellizzari and G. Wallace, *Rev. Geophys.*, 1983, **21**, 921–952.
- 3 J. Hoff, D. Mackay, R. Gillham and W. Shiu, *Environ. Sci. Technol.*, 1993, **27**, 2174–2180.
- 4 K. Hunter and P. Liss, *Mar. Chem.*, 1977, **5**, 361–379.
- 5 T. Novakov and J. Penner, *Nature*, 1993, **365**, 823–826.
- 6 H. Tervahattu, J. Juhanaja and K. Kupiainen, *J. Geophys. Res.-Atmos.*, 2002, **107**, 4319.
- 7 H. Tervahattu, J. Juhanaja, V. Vaida, A. Tuck, J. Niemi, K. Kupiainen, M. Kulmala and H. Vehkamaki, *J. Geophys. Res.-Atmos.*, 2005, **110**, D06207.
- 8 B. Mason, *Nature*, 1954, **174**, 470–471.
- 9 D. C. Blanchard, *Science*, 1964, **146**, 396.
- 10 Y. Jung and R. A. Marcus, *J. Am. Chem. Soc.*, 2007, **129**, 5492–5502.
- 11 O. Acevedo and K. Armacost, *J. Am. Chem. Soc.*, 2010, **132**, 1966–1975.
- 12 L. L. Thomas, J. Tirado-Rives and W. L. Jorgensen, *J. Am. Chem. Soc.*, 2010, **132**, 3097–3104.
- 13 V. Vaida, *J. Chem. Phys.*, 2011, **135**, 020901.
- 14 M. Boy, M. Kulmala, T. M. Ruuskanen, M. Pihlatie, A. Reissell, P. P. Aalto, P. Keronen, M. D. Maso, H. Hellen, H. Hakola, R. Jansson, M. Hanke and F. Arnold, *Atoms. Chem. Phys.*, 2005, **5**, 863–878.

- 15 L. Wang, A. F. Khalizov, J. Zheng, W. Xu, Y. Ma, V. Lal and R. Zhang, *Nat. Geosci.*, 2010, **3**, 031907.
- 16 J. Kirkby, J. Curtius, J. Almeida, E. Dunne, J. Duplissy, S. Ehrhart, A. Franchin, S. Gagné, L. Ickes, A. Kruten, A. Kupc, A. Metzger, F. Riccobono, L. Rondo, S. Schobesberger, G. Tsagkogeorgas, D. Wimmer, A. Amorim, F. Bianchi, M. Breitenlechner, A. David, J. Dommen, A. Downard, M. Ehn, R. C. Flagan, S. Haider, A. Hansel, D. Hauser, W. Jud, H. Junninen, F. Kreissl, A. Kvashin, A. Laaksonen, K. Lehtipalo, J. Lima, E. R. Lovejoy, V. Makhmutov, S. Mathot, J. Mikkil, P. Minginette, S. Mogo, T. Nieminen, A. Onnela, P. Pereira, T. Petj, R. Schnitzhofer, J. H. Seinfeld, M. Sipil, Y. Stozhkov, F. Stratmann, A. Tom, J. Vanhanen, Y. Viisanen, A. Vrtala, P. E. Wagner, H. Walther, E. Weingartner, H. Wex, P. M. Winkler, K. S. Carslaw, D. R. Worsnop, U. Baltensperger and M. Kulmala, *Nature*, 2011, **476**, 371–482.
- 17 R. Zhang, I. Suh, J. Zhao, D. Zhang, E. Fortner, X. Tie, L. Molina and M. Molina, *Science*, 2004, **304**, 1487–1490.
- 18 R. Zhang, L. Wang, A. F. Khalizov, J. Zhao, J. Zheng, R. L. McGraw and L. T. Molina, *Proc. Natl. Acad. Sci. U.S.A.*, 2009, **106**, 17650–17654.
- 19 A. Metzger, B. Verheggen, J. Dommen, J. Duplissy, A. S. H. Prevot, E. Weingartner, I. Riipinen, M. Kulmala, D. V. Spracklen, K. S. Carslaw and U. Baltensperger, *Proc. Natl. Acad. Sci. U.S.A.*, 2010, **107**, 6646–6651.
- 20 P. Gill, T. Graedel and C. Weschler, *Rev. Geophys.*, 1983, **21**, 903–920.
- 21 D. J. Donaldson and V. Vaida, *Chem. Rev.*, 2006, **106**, 1445–1461.
- 22 D. J. Donaldson and K. T. Valsaraj, *Environ. Sci. Technol.*, 2010, **44**, 865–873.
- 23 N. T. Southall, K. A. Dill and A. D. J. Haymet, *J. Phys. Chem. B.*, 2002, **106**, 521–533.
- 24 D. Chandler, *Nature*, 2005, **437**, 640–647.
- 25 B. Lee, *Biopolymers*, 1991, **31**, 993–1008.
- 26 S. Dixit, J. Crain, W. C. K. Poon, J. L. Finney and A. K. Soper, *Nature*, 2002, **416**, 829–832.
- 27 T. Sato, A. Chiba and R. Nozaki, *J. Chem. Phys.*, 1999, **110**, 2508–2521.
- 28 T. Sato, A. Chiba and R. Nozaki, *J. Chem. Phys.*, 2000, **112**, 2924–2932.
- 29 T. Sato, A. Chiba and R. Nozaki, *J. Chem. Phys.*, 2000, **113**, 9748–9758.
- 30 T. Sato and R. Buchner, *J. Chem. Phys.*, 2003, **118**, 4606–4613.
- 31 E. J. W. Wensink, A. C. Hoffmann, P. J. van Maaren and D. van der Spoel, *J. Chem. Phys.*, 2003, **119**, 7308–7317.
- 32 D. van der Spoel, P. J. van Maaren, P. Larsson and N. Timneanu, *J. Phys. Chem. B.*, 2006, **110**, 4393–4398.
- 33 D. van der Spoel, E. J. W. Wensink and A. C. Hoffmann, *Langmuir*, 2006, **22**, 5666–5672.
- 34 M. J. Krisch, R. D’Auria, M. A. Brown, D. J. Tobias, J. C. Hemminger, M. Ammann, D. E. Starr and H. Bluhm, *J. Phys. Chem. C*, 2007, **111**, 13497–13509.
- 35 M. Szori, M. Roeselova and P. Jedlovsky, *J. Phys. Chem. C*, 2011, **115**, 19165–19177.
- 36 C. Caleman and D. van der Spoel, *J. Chem. Phys.*, 2006, **125**, 154508.
- 37 C. Caleman and D. van der Spoel, *Phys. Chem. Chem. Phys.*, 2007, **9**, 5105–5111.
- 38 C. Caleman, J. S. Hub, P. J. van Maaren and D. van der Spoel, *Proc. Natl. Acad. Sci. U.S.A.*, 2011, **108**, 6838–6842.
- 39 D. E. Otten, P. R. Shaffer, P. L. Geissler and R. J. Saykally, *Proc. Natl. Acad. Sci. U.S.A.*, 2012, **109**, 701–705.
- 40 H. J. C. Berendsen, J. P. M. Postma, W. F. van Gunsteren and J. Hermans, *Intermolecular Forces*, D. Reidel Publishing Company, Dordrecht, 1981, pp. 331–342.
- 41 W. L. Jorgensen and J. Tirado-Rives, *Proc. Natl. Acad. Sci. U.S.A.*, 2005, **102**, 6665–6670.
- 42 H. J. C. Berendsen, J. R. Grigera and T. P. Straatsma, *J. Phys. Chem.*, 1987, **91**, 6269–6271.
- 43 W. L. Jorgensen, J. Chandrasekhar, J. D. Madura, R. W. Impey and M. L. Klein, *J. Chem. Phys.*, 1983, **79**, 926–935.
- 44 J. Wang, R. M. Wolf, J. W. Caldwell, P. A. Kollman and D. A. Case, *J. Comput. Chem.*, 2004, **25**, 1157–1174.
- 45 J. G. Kirkwood, *J. Chem. Phys.*, 1935, **3**, 300–313.
- 46 M. R. Shirts, J. W. Pitera, W. C. Swope and V. S. Pande, *J. Chem. Phys.*, 2003, **119**, 5740–5761.
- 47 W. L. Jorgensen, D. S. Maxwell and J. Tirado-Rives, *J. Am. Chem. Soc.*, 1996, **118**, 11225–11236.
- 48 G. A. Kaminski, R. A. Friesner, J. Tirado-Rives and W. L. Jorgensen, *J. Phys. Chem. B.*, 2001, **105**, 6474–6487.
- 49 B. Hess, *J. Chem. Phys.*, 2002, **116**, 209–217.
- 50 R. M. Neumann, *Am. J. Phys.*, 1980, **48**, 354–357.
- 51 D. van der Spoel, E. Lindahl, B. Hess, G. Groenhof, A. E. Mark and H. J. C. Berendsen, *J. Comput. Chem.*, 2005, **26**, 1701–1718.
- 52 B. Hess, C. Kutzner, D. van der Spoel and E. Lindahl, *J. Chem. Theory Comput.*, 2008, **4**, 435–447.
- 53 D. van der Spoel, P. J. van Maaren and C. Caleman, *Bioinformatics*, 2012, **28**, 752–753.
- 54 C. Caleman, P. J. van Maaren, M. Hong, J. S. Hub, L. T. Costa and D. van der Spoel, *J. Chem. Theory Comput.*, 2012, **8**, 61–74.
- 55 H. J. C. Berendsen and W. F. van Gunsteren, *Molecular-Dynamics Simulation of Statistical-Mechanical Systems*, Amsterdam, 1986, pp. 43–65.
- 56 W. F. van Gunsteren and H. J. C. Berendsen, *Mol. Sim.*, 1988, **1**, 173–185.
- 57 S. Miyamoto and P. A. Kollman, *J. Comput. Chem.*, 1992, **13**, 952–962.
- 58 B. Hess, *J. Chem. Theory Comput.*, 2008, **4**, 116–122.
- 59 A. V. Marenich, C. P. Kelly, J. D. Thompson, G. D. Hawkins, C. C. Chambers, D. J. Giesen, P. Winget, C. J. Cramer and D. G. Truhlar, *Minnesota Solvation Database version 2009*, University of Minnesota, Minneapolis, U.S.A., 2009.
- 60 K. Lum, D. Chandler and J. Weeks, *J. Phys. Chem. B*, 1999, **103**, 4570–4577.
- 61 R. R. Netz and D. Horinek, *Annu. Rev. Phys. Chem.*, 2012, **63**, 401–418.
- 62 H.-A. Yu and M. Karplus, *J. Chem. Phys.*, 1988, **89**, 2366–2379.
- 63 K. Lum, D. Chandler and J. Weeks, *JOURNAL OF PHYSICAL CHEMISTRY B*, 1999, **103**, 4570–4577.
- 64 B. Mmerekki and D. Donaldson, *J. Phys. Chem. A*, 2003, **107**, 11038–11042.
- 65 B. Mmerekki, D. Donaldson, J. Gilman, T. Eliason and V. Vaida, *Atmos. Environ.*, 2004, **38**, 6091–6103.
- 66 B. J. Finlayson-Pitts, *Phys. Chem. Chem. Phys.*, 2009, **11**, 7760–7779.
- 67 J. B. Fenn, M. Mann, C. K. Meng, S. F. Wong and C. M. Whitehouse, *Science*, 1989, **246**, 64–71.
- 68 A. Patriksson, E. Marklund and D. van der Spoel, *Biochemistry*, 2007, **46**, 933–945.
- 69 E. G. Marklund, D. S. D. Larsson, D. van der Spoel, A. Patriksson and C. Caleman, *Phys. Chem. Chem. Phys.*, 2009, **11**, 8069–8078.
- 70 D. van der Spoel, E. G. Marklund, D. S. D. Larsson and C. Caleman, *Macromol. Biosci.*, 2011, **11**, 50–59.
- 71 Y. Wang, D. S. D. Larsson and D. van der Spoel, *Biochemistry*, 2009, **48**, 1006–1015.
- 72 R. Friemann, D. S. D. Larsson, Y. Wang and D. van der Spoel, *J. Am. Chem. Soc.*, 2009, **131**, 16606–16607.
- 73 L. Konermann, *J. Phys. Chem. B*, 2007, **111**, 6534–6543.
- 74 E. Ahadi and L. Konermann, *J. Am. Chem. Soc.*, 2010, **132**, 11270–11277.
- 75 E. Ahadi and L. Konermann, *J. Phys. Chem. B*, 2012, **116**, 104–112.
- 76 M. Dole, L. Mack and R. Hines, *J. Chem. Phys.*, 1968, **49**, 2240–&.
- 77 P. Kebarle and U. H. Verkerk, *Mass Spectrom. Rev.*, 2009, **28**, 898–917.
- 78 R. Neutze, R. Wouts, D. van der Spoel, E. Weckert and J. Hajdu, *Nature*, 2000, **406**, 752–757.
- 79 S. P. Hau-Riege, R. A. London, H. N. Chapman, A. Szöke and N. Timneanu, *Phys. Rev. Lett.*, 2007, **98**, 198302.
- 80 N. Timneanu, C. Caleman, J. Hajdu and D. van der Spoel, *Chem. Phys.*, 2004, **299**, 277–283.